Noname manuscript No.
(will be inserted by the editor)

Methods for Geometrical Video Projector Calibration

Jamil Draréni · Sébastien Roy · Peter Sturm

Received: date / Accepted: date

Abstract In this paper we present two methods to geometrically calibrate a video projector using a markerless planar surface. The first method assumes a partial knowledge on the camera parameters whereas the second method consists in an auto-calibration method with no assumption on the parameters of the camera. Instead, the auto-calibration is performed by identifying a roughly fronto-parallel pose of the camera w.r.t the projection surface.

The fact that camera calibration is not needed increases the usability of the methods and at the same time eliminates one potential source of inaccuracy, since errors in the camera calibration would otherwise inevitably propagate through the projector calibration. Not using a printed pattern as most existing methods do is another gain in accuracy and ease of use.

As depicted by our experiments,both methods enjoy a good stability and give good results when compared against existing methods.

Keywords Video Projector Calibration · Planar Calibration · Auto-Calibration · focal estimation · Structured Light · Photometric Stereo.

1 Introduction

With the recent advances in projection display, video projectors are becoming the devices of choice for active reconstruction systems and 3D measurement. Such systems like Structured Light [19] and also Photometric Stereo [24,2] use video projectors to alleviate the difficult task of establishing point correspondences. However, even if active systems can solve the matching problem, the calibration of video projectors is still required. In fact, as in any stereo setup, the intrinsic calibration is the key to an euclidean reconstruction or to estimate the projector's orientation when the latter is used as an illumination device (for a photometric stereo system).

J. Draréni , S. Roy
DIRO, Université de Montréal.
E-mail: {drarenij,roys}@iro.umontreal.ca

P. Sturm
INRIA Rhône-Alpes.
E-mail: Peter.Sturm@inrialpes.fr

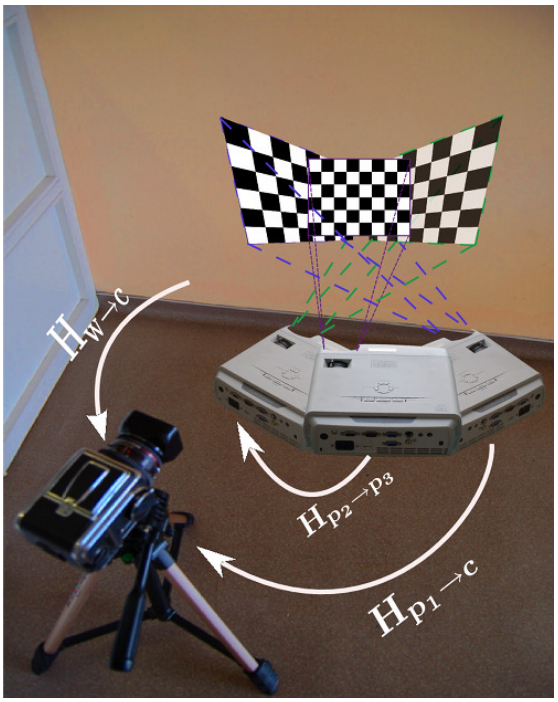

Fig. 1 A Camera-Projector setup and its homographies (see text).

The projection model carried out by a video projector is usually modeled as the inverse projection of a pin-hole camera, and thus considered as a perspective projection.

In order to simplify the calibration process, a planar surface is often used as projection surface, onto which features or codified patterns are projected. The way patterns are codified and the projection surface orientation is estimated distinguishes most previous calibration methods from one another.

In [20,22], a video projector projects patterns on a plane mounted on a mechanically controlled platform. Thus, the orientation and position of the projection plane is known and is used to calibrate the structured light system using conventional camera calibration techniques.

For convenience and because the projection surface is usually planar, we will also refer to it as the *wall*.

In [18], a planar calibration grid is attached to the wall and observed by a calibrated camera. Due to the camera's calibration information and the metric information about the grid, the grid's and thus the wall's orientation and distance relative to the camera can be computed by classical pose estimation. After this, the 3D positions of features projected onto the wall by the video projector, can be easily computed. If this is done for three or more positions of the video projector, a set of correspondences between the wall and the "projector images" can be obtained and then used to estimate the projector parameters with standard plane-based calibration methods [21,26]. We refer to this method as Direct Linear Calibration (DLC). Note that all this could actually be done without pre-calibrating the camera, purely based on plane homographies, as explained in section 2.1. Further, to in-

crease accuracy of the DLC, a printed planar target with circular markers is used in [16], to calibrate the camera as well as the projector.

In [9], a structured light system is calibrated without using a camera. This is made possible by embedding light sensors in the target surface (the wall). Gray-coded binary patterns are then projected to estimate the sensor locations and prewarp the image to accurately fit the physical features of the projection surface. The projector parameters are not explicitly estimated but the method could easily be extended for that purpose.

In [17], an auto-calibration method for multi-projector display walls is proposed. The authors focus more on estimating the relative orientations of the projectors w.r.t a camera to achieve a large seamless display. The method does not require fiducial points but makes assumptions on the projector intrinsic parameters and the camera must be calibrated. Further, the method assumes the x-axis of the projectors aligned.

Okatani *et al*. [15] presented a work on video projector auto-calibration but their work is meant for multiple projectors alignment and keystoning provided that the intrinsic parameters of the projectors are known.

Kimura *et al*. [7] proposed a calibration method based on the camera-projector epipolar geometry. Again, the camera must be fully calibrated.

More recently, Audet *et al*. [1] presented a new method for video projector calibration. It uses printed tags on a planar surface to infer the orientation of the surface before performing a classical plane-based calibration. In this system the captured tags are reprojected and imaged again by the camera. The orientation is refined by minimizing the reprojection error. This is a tedious and error-prone task especially because the planar surface is hand held.

In this paper, we present two methods to calibrate a video projector. As opposed to most existing methods, the proposed methods do not require a physical calibration grid. The first method overcomes the problem of determining the camera-wall homography $\mathsf{H}_{w\to c}$ by exploring the space of all acceptable homographies and consider the one that minimizes the reprojection error (see Figure.1). Since $\mathsf{H}_{w\to c}$ depends only on the orientation between the camera and the wall, the space of acceptable homographies can be parameterized with only 2 angles: the elevation and the azimuth angles that define the normal vector at the wall.

Finding the normal of the wall consists then in sampling the space of orientations on a unit sphere. For each candidate we perform a classical plane-based calibration and consider the one that minimizes the reprojection error. We call this method orientation sampling calibration.

The second method instead imposes only two constraints on the calibration setup. Namely, the camera should remain static while the video projector displays patterns onto a planar surface and the user must put the projector once in a roughly fronto-parallel position relative to the wall. The latter constraint does not have to be exact and serves only as a starting point for a non-linear minimization as explained later. We refer to this method as video-projector auto-calibration.

The rest of the paper is organized as follows. In section 2 we introduce our projector model and the above mentioned DLC (direct linear calibration) approach, which serves as an introduction to the proposed methods.

The orientation sampling calibration and the auto-calibration described are presented in section 3 and 4 respectively. Experimental results are depicted in section 5 and conclusions are drawn in section 6.

2 Projector Model

Throughout this paper, the projector is assumed to have a perspective projection model like a pin-hole camera, with the slight difference that here the projection direction is reversed [7]. Based on this assumption, a 3D point $P = [X, Y, Z, 1]^\mathsf{T}$ is mapped to $p_p = [x, y, 1]^\mathsf{T}$ in the projector as:

$$p_p \sim \mathsf{K}_p \left(\mathsf{R}_p \ \mathbf{t}_p\right) P \tag{1}$$

where $\sim$ stands for equality up to scale between homogeneous coordinates. These 2D points p_p live in what we refer to by the "projector image".

The matrix R_p and the vector $\mathbf{t}_p$ represent the extrinsic parameters of the projector. The calibration matrix K_p is described by the sought internal parameters and is defined as follows:

$$\mathsf{K}_p = \begin{pmatrix} \rho f & 0 & u_0 \\ 0 & f & v_0 \\ 0 & 0 & 1 \end{pmatrix} \tag{2}$$

where f, ρ and (u, v) are respectively the focal length, the aspect ratio and the principal point coordinates.

Consider a camera imaging what is projected by the projector onto the wall. Since we assume the wall to be planar, it induces an homography $\mathsf{H}_{p\to c}$ between the projector and the camera image. Without loss of generality, we may assume that the world coordinate system is aligned with the wall, such that points on the wall have coordinates $Z = 0$. Then, the homography between projector and camera can be written as:

$$\mathsf{H}_{p\to c} \sim \underbrace{\mathsf{K}_c \left(\bar{\mathsf{R}}_c \ \mathbf{t}_c\right)}_{\mathsf{H}_{w\to c}} \underbrace{\left(\mathsf{K}_p \left(\bar{\mathsf{R}}_p \ \mathbf{t}_p\right)\right)^{-1}}_{\mathsf{H}_{p\to w}} \tag{3}$$

where $\bar{\mathsf{A}}$ refers to the first two columns of a 3×3 matrix A. K_c is the camera's calibration matrix and R_c and $\mathbf{t}_c$ represent its extrinsic parameters. The homography $\mathsf{H}_{p\to c}$ can also be seen as the product of the homography $\mathsf{H}_{p\to w}$ that maps the projector image plane to the wall with $\mathsf{H}_{w\to c}$, the homography that relates the wall to the camera image plane.

2.1 The Direct Linear Calibration

In this section, we review the details of the Direct Linear Calibration for projectors. This method is used as a reference for our experiments. As opposed to [18], the variant presented here [3] is strictly based on homographies and does not require a calibrated camera.

A planar calibration grid is attached to the wall. This allows to estimate the homography $\mathsf{H}_{w\to c}$ between the wall and the camera, introduced above. It relates a point p_w on the wall to a point p_c in the camera image as follows:

$$p_c \sim \mathsf{H}_{w\to c} p_w \tag{4}$$

Once this homography is computed (details on homography estimation can be found in [5]), the video projector is used to project patterns while it is moved to various positions and orientations. For each projector pose i, correspondences are established between the camera

and the video projector, leading to an homography $\mathsf{H}_{c\to p_i}$. A point p_c in the camera image is mapped into the projector at pose i as:

$$p_p^i \sim \mathsf{H}_{c\to p_i} p_c \tag{5}$$

Combining (4) and (5), a point p_w on the wall is mapped into the i^{th} projector as:

$$p_p^i \sim \underbrace{\mathsf{H}_{c\to p_i}\mathsf{H}_{w\to c}}_{\mathsf{H}_{w\to p_i}} p_w \tag{6}$$

We thus can compute the wall-to-projector homography for each pose i. It has the following form (see above):

$$\mathsf{H}_{w\to p_i} \sim \mathsf{K}_p \left(\bar{\mathsf{R}}_p^i \ \mathbf{t}_p^i\right) \tag{7}$$

It is now straightforward to apply classical plane-based calibration methods [21,26] to calibrate the projector and, if necessary, to compute its extrinsic parameters, from two or more poses.

3 Orientation Sampling Calibration

In this section we give the details of the first method for video projector calibration. As discussed earlier in the introduction, the justification for using an attached calibration rig to the wall is to infer the homography *wall-camera* in order to estimate the 3D coordinates of the projected features. We propose to estimate this *wall-camera* relation by exploring the space of all possible orientations since only the orientation of the wall w.r.t the camera matters and not its position.

The calibration process can be outlined in three main steps:

- Pick a wall direction candidate , d_i.
- Compute H_i,the homography associated to d_i.
- Use H_i to perform a DLC calibration (Section 2.1).

The above steps are repeated for all possible wall directions (d_i). and the direction that minimizes the reprojection errors is selected as the correct plane orientation. The first two steps are detailed in the next subsections. The third one is straightforward from section 2.1.

3.1 Orientation Selection

In this part we present our approach for selecting wall directions uniformly. This problem is closely related to the problem of uniformly generating samples on a unit sphere which is also known as *sphere point picking problem*.

It is well known that uniformly selected spherical coordinates $\theta \in [0, 2\pi]$ and $\phi \in [0, \pi]$ do not generate uniform points on a sphere. This is because the area element spanned by θ and ϕ is $d\Omega = \sin\phi d\theta d\phi$ and is function of ϕ. Hence, the points distribution will be denser near the poles.

To uniformly sample a sphere one could use either a random or a deterministic strategy [25]. The first class methods consist of randomly generating points in a volume, followed by

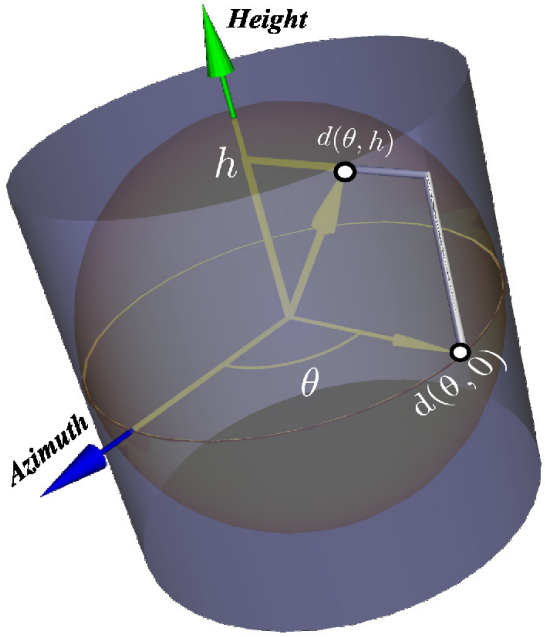

Fig. 2 Orientation space sampling. A point on the unit cylinder is uniformly chosen by uniformly picking an azimuth angle (θ) and a height (h). The resulting direction $d(\theta, h$ is then axially projected on the unit sphere.

an acceptance/rejection step depending on whether the points lie or not on the sphere. The randomness of the selection makes it hard to bound the running time of these methods.

Instead, deterministic methods produce valid samples on a unit sphere from uniformly distributed parameters, such methods include (but not limited to) quaternion sampling [6], normal-deviate methods [8] and trigonometric methods [13, 12, 14].

From the latter category, we chose to use the one based on Archimedes theorem [13] for its simplicity and efficiency. As the name suggests, this method is based on Archimedes theorem on the sphere and cylinder which states that the area of a sphere equals the area of every right circular cylinder circumscribed about the sphere excluding the bases. This argument leads naturally to a simple sphere sampling algorithm based on cylinder sampling and was introduced in [13]. The outline of the aforementioned method is as follow.

Uniformly sampled points on a cylinder are first generated by picking an azimuth angle $\theta_i \in [0, \pi]$ and a height $h_i \in [-1, +1]$ uniformly, resulting in direction vectors $d(\theta_i, h_i)$.

The vectors $d(\theta_i, h_i)$ are then axially projected on the unit sphere using standard trigonometric identities and the result are uniform samples on the sphere (See Figure.2)

In our case, we only need to sample the directions on the hemisphere facing the camera. Thus the range of the parameters h and θ is limited to $[-1, +1] \times [0, \pi]$.

3.2 Homography From an Orientation Sample

The homography wall-camera $\mathsf{H}^i_{w\to c}$ induced by a wall whose normal is given by $\mathbf{d}_i$ (see previous subsection), is defined by:

$$\mathsf{H}^i_{w\to c} \sim \mathsf{K}_{cam}.\left[\mathbf{R}^i_1\mathbf{R}^i_2\mathbf{t}\right] \tag{8}$$

Where K_{cam}, $\mathbf{R}^i_1$, $\mathbf{R}^i_2$ and $\mathbf{t}$ are respectively the intrinsic camera matrix, the first two vectors of the rotation which depend on $\mathbf{d}_i$ and the translation vector. Without loss of generality and for the sake of simplicity, we fix the projection of the origin of the wall $P^0_w = (0,0)^\mathsf{T}$ in the camera at the image center. With this convention, the translation vector $\mathbf{t}$ simplifies to $(0,0,1)^\mathsf{T}$.

The rotation matrix R^i is derived from $\mathbf{d}_i$ via Rodrigues formula, which requires a rotation axis and a rotation angle. The rotation axis is simply the result of the cross product between $\mathbf{d}_i$ and the vector $(0,0,1)^\mathsf{T}$ whereas the rotation angle α_i is obtained from the dot product of the same vectors:

$$\alpha_i = \mathbf{cos^{-1}}\left({\mathbf{d}_i}^\mathsf{T} \cdot (0,0,1)^\mathsf{T}\right) \tag{9}$$

3.3 Complete Algorithm

We are now ready to give the complete algorithm of our video projector calibration. We assume the existence of two supporting functions, *ReprojError* that returns a reprojection error for a given projector parameters and *DLC* a function that estimate the projector parameters using the DLC method (see Section.2.1).

Algorithm 1: Orientation Sampling Calibration

Data: $\mathsf{H}^k_{c\to p}$, the k camera-projector homographies and K_{cam} Camera intrinsic matrix (optional).
foreach $(h_i,\theta_i)\in[-1,1]\times[-\pi/2,\pi/2]$, f_i **do**
  Estimate direction $\mathbf{d}_i(\theta_i,h_i)$ (sec.3.1);
  if K_{cam} *is undef* **then**
    Initialize elements of K_{cam} using image center and f_i;
  end
  Estimate $\mathsf{H}^i_{w\to c}$ from $\mathbf{d}_i$ and f_i (sec.3.2);
  foreach $\mathsf{H}^k_{c\to p}$ **do**
    $\mathsf{H}^k_{w\to p} = \mathsf{H}^k_{c\to p}\cdot\mathsf{H}^i_{w\to c}$;
  end
  $\mathsf{K}^i_{proj} \leftarrow$ `DLC(`$\mathsf{H}^k_{c\to p}$`)` (sec.2.1) ;
  Error $\leftarrow$ `ReprojError(`K^i_{proj}`)` ;
  if Error $<$ BestError **then**
    $\mathsf{K}_{proj} \leftarrow \mathsf{K}^i_{proj}$;
    BestError $\leftarrow$ Error;
  end
end
return *Projector calibration matrix* K_{proj}

No range has been specified for the focal length values f_i. In theory, one can use a large range which, in practice, could be narrowed based on informations given by the manufacturer. In all our tests, focal range was set to $[10^2, 10^4]$.

The algorithm selects the normal that minimizes the reprojection error. This error function is undoubtedly prone to local minima. But this is not an issue in our case because no gradient-based optimization was used. It is worth noting that the real normal of the wall is not the only solution that minimizes the reprojection error. The mirror normal also does. But, since we sample a hemisphere, the algorithm visits only normals pointing toward the camera thus, the uniqueness of the solution is guaranteed.

4 Projector Auto-Calibration

The method presented in the previous section, yet simple, imposes a constraint on the camera's intrinsics. Namely, the principal point is assumed to be at the center of the image.

In this section, we show that this requirement may be avoided and propose a true geometric video projector auto-calibration method. This means that not only the camera calibration is unnecessary but nor the metric of the scene.

4.1 Basic Idea

The key observation underlying the auto-calibration approach is as follows. It is "easy" to compute homographies between the projector image and the camera image, induced by the projection surface. There are indeed many possibilities to do so, the simplest ones consisting in projecting a single pattern such as a checkerboard and extracting and identifying corners in the camera image. More involved ones could make use of multiple patterns, sequentially projected from each considered projector pose, such as Gray codes, allowing for robust and dense matching. From the obtained matches, the computation of the homography is straightforward.

Consider now homographies associated with two poses of the projector, $\mathsf{H}_{c\to p_i}$ and $\mathsf{H}_{c\to p_j}$. From these we can compute an homography between the two projector images, induced by the planar projection surface:

$$\begin{aligned}\mathsf{H}_{p_i\to p_j} &\sim \mathsf{H}_{w\to p_j}\mathsf{H}_{w\to p_i}^{-1}\\ &\sim \mathsf{H}_{c\to p_j}\mathsf{H}_{w\to c}\left(\mathsf{H}_{c\to p_i}\mathsf{H}_{w\to c}\right)^{-1}\\ &\sim \mathsf{H}_{c\to p_j}\mathsf{H}_{c\to p_i}^{-1}\end{aligned}$$

We are now in the exact same situation as an uncalibrated perspective camera taking images of an unknown planar scene: from point matches, the associated plane homographies can be computed and it is well-known that camera auto-calibration is possible from these, as first shown by Triggs [23]. We may thus apply any existing plane-based auto-calibration method, e.g. [23,11,4] to calibrate the projector. Compared to auto-calibration of cameras, the case of projectors has an advantage; many and highly accurate point matches can be obtained since the scene texture is controlled, by projecting adequate patterns onto the wall.

Plane-based auto-calibration comes down to a non-linear optimization problem, even in the simplest case when only the focal length is unknown. To avoid convergence problems, we adopt an approach suggested in [4] that requires to take one image in a roughly fronto-parallel position relative to the scene plane. Here, this means of course by analogy that the projector should once be positioned in a roughly fronto-parallel position relative to the wall; subsequent poses can (and should) then be different. This allows for a closed-form initial solution to the auto-calibration problem, which may then be refined by a non-linear

optimization (bundle adjustment). Note that the assumption of fronto-parallelism for one of the images is only required for the initialization; during optimization, this is then no longer enforced.

4.2 Initialization Procedure

We derive the initialization procedure in a different and simpler way compared to [4]. Let the fronto-parallel view correspond to pose 1; in the following we only consider homographies between that view and all the others. Consider first the wall-to-projector homography of the fronto-parallel view, $\mathsf{H}_{w\to p_1}$. So far, we have assumed that the world coordinate system is such that the wall is the plane $Z = 0$ (see section 2). Without loss of generality, we may assume that the X and Y axes are aligned with those of the fronto-parallel view and that the optical center of that view is located at a distance equal to 1 from the wall. Note that these assumptions are not required to obtain the below results, but they simply make the formulae simpler. With these assumptions, the wall-to-projector homography for the fronto-parallel pose is simply:

$$\mathsf{H}_{w\to p_1} \sim \mathsf{K}_p$$

Consider now the homography between the fronto-parallel view and another view j:

$$\begin{aligned}\mathsf{H}_{p_1\to p_j} &\sim \mathsf{H}_{w\to p_j}\mathsf{H}_{w\to p_1}^{-1}\\ &\sim \mathsf{K}_p\left(\bar{\mathsf{R}}_p^j\ \mathbf{t}_p^j\right)\mathsf{K}_p^{-1}\end{aligned}$$

In the following let us, for simplicity, drop all indices:

$$\mathsf{H} \sim \mathsf{K}\left(\bar{\mathsf{R}}\ \mathbf{t}\right)\mathsf{K}^{-1}$$

It follows that:

$$\mathsf{K}^{-1}\mathsf{H} \sim \left(\bar{\mathsf{R}}\ \mathbf{t}\right)\mathsf{K}^{-1}$$

Let us now multiply each side of the equation from the left with its own transpose:

$$\mathsf{H}^T\mathsf{K}^{-T}\mathsf{K}^{-1}\mathsf{H} \sim \mathsf{K}^{-T}\left(\bar{\mathsf{R}}\ \mathbf{t}\right)^T\left(\bar{\mathsf{R}}\ \mathbf{t}\right)\mathsf{K}^{-1}$$

Since $\bar{\mathsf{R}}$ consists of the first two columns of the rotation matrix R, we have $\bar{\mathsf{R}}^T\bar{\mathsf{R}} = \mathtt{I}$ and thus:

$$\mathsf{H}^T\mathsf{K}^{-T}\mathsf{K}^{-1}\mathsf{H} \sim \mathsf{K}^{-T}\begin{pmatrix}1 & 0 & \times\\ 0 & 1 & \times\\ \times & \times & \times\end{pmatrix}\mathsf{K}^{-1}$$

where entries marked as $\times$ depend on $\mathbf{t}$ and are irrelevant for the following. Due to the form of K, this becomes:

$$\mathsf{H}^T\mathsf{K}^{-T}\mathsf{K}^{-1}\mathsf{H} \sim \begin{pmatrix}1 & 0 & \times\\ 0 & \rho^2 & \times\\ \times & \times & \times\end{pmatrix} \tag{10}$$

Let us use the image of the absolute conic (IAC) to parameterize the projector's intrinsic parameters, defined as $\omega \sim \mathsf{K}^{-T}\mathsf{K}^{-1}$. From (10) we can now deduce the following two equations on the intrinsic parameters, which are similar to those of calibration based on a planar calibration grid [21,26]:

$$h_1^T\omega h_2 = 0 \tag{11}$$

$$\rho^2 h_1^T\omega h_1 - h_2^T\omega h_2 = 0 \tag{12}$$

where h_k denotes the kth column of H. Let us note that $\rho^2 = \omega_{11}/\omega_{22}$; hence, equation (12) can be written:

$$\omega_{11} h_1^T \omega h_1 - \omega_{22} h_2^T \omega h_2 = 0 \tag{13}$$

Equation (11) is linear in ω, whereas (13) is quadratic. There are different ways of using these equations to compute the IAC ω and from this, the intrinsic parameters. If the aspect ratio ρ is known beforehand, both equations are linear and thus easy to solve. If ρ is unknown, one can either use only the linear equation (11), which requires five views (the fronto-parallel one and four others), or compute ω from three views only. In the latter case, we have two linear and two quadratic equations and a "closed-form" solution in the form of a degree-4 polynomial in one of the unknowns, is straightforward to obtain.

4.3 Non-linear Optimization

Once an initial solution of the projector calibration is computed using the above approach, a non-linear optimization through bundle adjustment may be carried out. Let us briefly outline its peculiarities, compared to plane-based auto-calibration of a camera. Note that the only noisy observations in our scenario are features in the camera image: those in the projector "images" are perfectly known and noisefree! Hence, the cost function of the bundle adjustment should be based on the reprojection error in the camera image. The following formulation is one possible option:

$$\min_{\mathsf{H}_{w\to c}, \mathsf{K}_p, \mathsf{R}_p^i, \mathbf{t}_p^i} \sum_{i,j} dist^2 \left(p_c^{ij}, \mathsf{H}_{w\to c} \mathsf{H}_{p_i \to w} p_p^{ij} \right)$$

where i stands for projector poses and j for points. I.e. we optimize the wall-to-camera homography, the intrinsic projector parameters and its extrinsic parameters for all views, by minimizing the reprojection error when mapping from the projector images into the camera image (the $\mathsf{H}_{p_i\to w}$ are parameterized by K_p and the extrinsic projector parameters).

Another option would be to include camera intrinsics and extrinsics in the optimization instead of the "black-box" homography $\mathsf{H}_{w\to c}$, but since the camera is static in our case, at most two intrinsics can be estimated [21, 26].

Let us briefly describe the gauge freedom in our problem. Everything is defined up to a 3D similarity transformation, i.e. 7 degrees of freedom (rotation, translation, and scale). We fix 3 of those by letting the projector screen be the plane $Z = 0$. We may fix 3 others by imposing an arbitrary position for one of the projector images. The remaining degree of freedom corresponds to rotation about the normal of the projector screen. This may be fixed by imposing e.g. an X-coordinate of the position of a second projector image.

Overall, for n projector images, we thus have $8 + m + 6n - 4$ parameters to optimize, where m is the number of estimated projector intrinsics (usually, 3) and the 8 correspond to the coefficients of the wall-to-camera homography.

In our implementation, we use the Levenberg-Marquardt method for the optimization and make use, as is common practice, of the sparsity of the problem's normal equations. At each iteration, solving the normal equations comes down to inverting 6×6 symmetric matrices (blocks corresponding to extrinsic parameters of individual projector images), and inverting one 11×11 symmetric matrix (a block corresponding to homography and intrinsic parameters). The whole bundle adjustment takes far less than a second on a standard PC.

We have not talked about radial distortion correction in this paper for two reasons. First, most video projectors will exhibit little if any radial distortions because they were specifically designed to render aesthetically pleasing videos (home theater, for instance). The second reason is simply due to the fact that, once the projectors pose recovered and 3D positions of feature points estimated, one can apply any classical method for camera radial distortion removal.

4.4 Estimation of Focal Length Changes

The above paragraphs constitute our auto-calibration approach. Here, we describe another method that allows to estimate the change of the projector's intrinsics caused by zooming. If the projector has been calibrated beforehand, this allows to update its calibration. We suppose that a zoom causes, besides the focal length, also the principal point to change (especially its vertical coordinates is likely to change in practice), but that the aspect ratio ρ remains constant.

We also suppose here that both the camera and the projector remain static. Let H be the projector-to-camera homography before zooming and H' the one afterwards. The inter-image homography between the two projector images is then given by:

$$\begin{aligned}\mathsf{M} &\sim \left(\mathsf{H}'\right)^{-1}\mathsf{H} \\ &\sim \mathsf{K}'_p\left(\mathsf{K}_p\right)^{-1} \\ &\sim \begin{pmatrix} f' & 0 & u'f - uf' \\ 0 & f' & v'f - vf' \\ 0 & 0 & f \end{pmatrix}\end{aligned}$$

It is straightforward to compute the intrinsic parameters after zooming:

$$\begin{aligned} f' &= \frac{M_{11}}{M_{33}}f \\ u' &= \frac{M_{13} + uM_{11}}{M_{33}} \\ v' &= \frac{M_{23} + vM_{11}}{M_{33}}\end{aligned}$$

Note that M depends only on the three unknown intrinsic in K'_p and can thus be computed from two points matches already. If the principal point can be assumed to remain constant, a single match is sufficient. A single match is also sufficient if only one coordinate of the principal point is supposed to change due to zooming (which is often the case for video projectors).

5 Experiments

We will now present the results of the experiments performed in order to assess the quality of the proposed methods. For the orientation sampling method (see section 3) we only performed tests on real data. This is because the core method is identical to the classical plane-based calibration [21,26]. However, we tested the auto-calibration method (see section 4) on both synthetic and real data.

For the real experiments, both method were fed with images shot with a Nikon D50 operating at a resolution of 1500×1000. The video projector is a Mitsubishi pocket projector of 800×600 pixels resolution.

Also, to include the DLC algorithm (see section 2.1) in our benchmarks, the camera was mounted on a tripod and was first registered to the wall using an attached printed chessboard. Images of projected chessboard using the video projector under several orientations were then acquired using the camera.

We took precaution to remove the attached chessboard form the wall before acquiring the projector images to avoid overlaps between the projected patterns and the rigidly attached pattern.

5.1 Orientation Sampling (Real Experiments)

The Orientation Sampling method was tested with both a calibrated and an uncalibrated camera.In the first case, we used the image of the attached checker to infer the wall-camera homography and calibrated as explained in Section.3. For the second method, we used a multi-resolution strategy to sample the azimuth angles and heights. The conditions of the third me- thod were identical to the second one except that the camera parameters were ignored and were estimated as follows :

- The focal length (of the camera) estimation was included in the sampling process. The sampling range was $[0, 10000]$.
- The pixels are assumed square.
- The center of projection is assumed to coincides with the image center.

Table 1 Projector calibration benchmark: Direct method, Orientation sampling with a calibrated camera (Sampling-C) and Orientation sampling with an uncalibrated camera (Sampling-U).

Method	$\mathbf{f_{proj}}$	ρ	$\mathbf{u_0}$	$\mathbf{v_0}$	$\mathbf{f_{cam}}$	**Error**	**Error B.A**	**Time (sec)**
Direct	1320.13	1.02	382.1	368	-	4.35	0.47	0.18
Sampling-C	1327.30	1.01	377.4	366	-	0.43	0.22	1.23
Sampling-U	1322.15	1.00	376	360	3108	0.16	0.09	6.2

The result of this benchmark is outlined on the Table 1. The latter depicts the estimated parameters, the reprojection errors in pixels (*Error*), and the error difference comparing before and after applying a bundle adjustment refinement (*Error B.A*). Technical and implementation details on bundle adjustment can be found in [10].

From this test, we can see that our method, even in the absence of camera parameters knowledge, out-perform the Direct Linear Method at the expenses of a higher running time. However, we are convinced that the performance of our implementation could be further improved by choosing a better multi-scale sampling strategy. We also consider that not requiring a printed chessboard attached to the wall is a major advantage, especially when the wall surface is large or not accessible.

5.2 Auto-Calibration (Synthetic Experiments)

We performed several tests on the auto-calibration method using synthetic data to assess its sensitivity to noise, number of projector poses and fronto-parallelism inaccuracy. Through-

out all the synthetic experiments, we used a camera panned at 30 degrees w.r.t the projection surface. The camera resolution was set to 1000×1000 and its calibration matrix defined as:

$$\mathsf{K}_c = \begin{pmatrix} 1000 & 0 & 500 \\ 0 & 1000 & 500 \\ 0 & 0 & 1 \end{pmatrix} \tag{14}$$

The projector parameters are identical to the camera parameters. A brief description of the tests follows:

Sensitivity to noise level. Here we added a zero-mean gaussian noise to the features imaged by the virtual camera.

Sensitivity to the number of projector poses. Here the amount of noise was fixed to $\sigma = 1$ and we varied the number of projector's poses from 2 to 20.

Sensitivity to fronto-parallelism inaccuracy. For this test, the coordinates were added a noise of 0.5 and we altered the orientation of the fronto-parallel pose by different amounts.

The results of these tests are depicted on Figure 3.

5.3 Auto-Calibration (Real Experiments)

To assess the auto-calibration method we used the same set of images as before. However, we manually identified a set of images where the projector was fronto-parallel to the wall. Note that this procedure could be achieved automatically as fronto-parallel homographies have a special form.

Table 2 Projector calibration benchmark: Direct method and the proposed Auto-Calibration method.

Method	$\mathbf{f_{proj}}$	ρ	$\mathbf{u_0}$	$\mathbf{v_0}$	**Error**
DLC	1320.13	1.002	382.1	448	0.46
Auto-Calib	1312.27	1.007	370.28	466	$0.42 - 0.27$

The results are outlined on the Table 2. The table provides the estimated parameters and the reprojection error in pixels. Because our method was initialized with several fronto-parallel images we reported the range of reprojection error instead of an error average. Again, the results of the DLC method are reported for comparaison.

We performed a second calibration test on a video projector (Mitsubishi XD430U) with a zooming capability and a native resolution of 1024×768. For this test, we estimated the intrinsic parameters with two different zoom settings and the results were compared to the predictions obtained using the method introduced in section 4.4.

We observed that both methods are consistent as reported in Table 3.

Table 3 Calibration results with varying parameters.

Method	$\mathbf{f_{proj}}$	ρ	$\mathbf{u_0}$	$\mathbf{v_0}$
Zoom 1	2292.29	1.045	584.42	969.36
Zoom 2 (pred)	1885.7	1.045	587.64	949.55
Zoom 2 (est)	1873.14	1.045	590.9	944

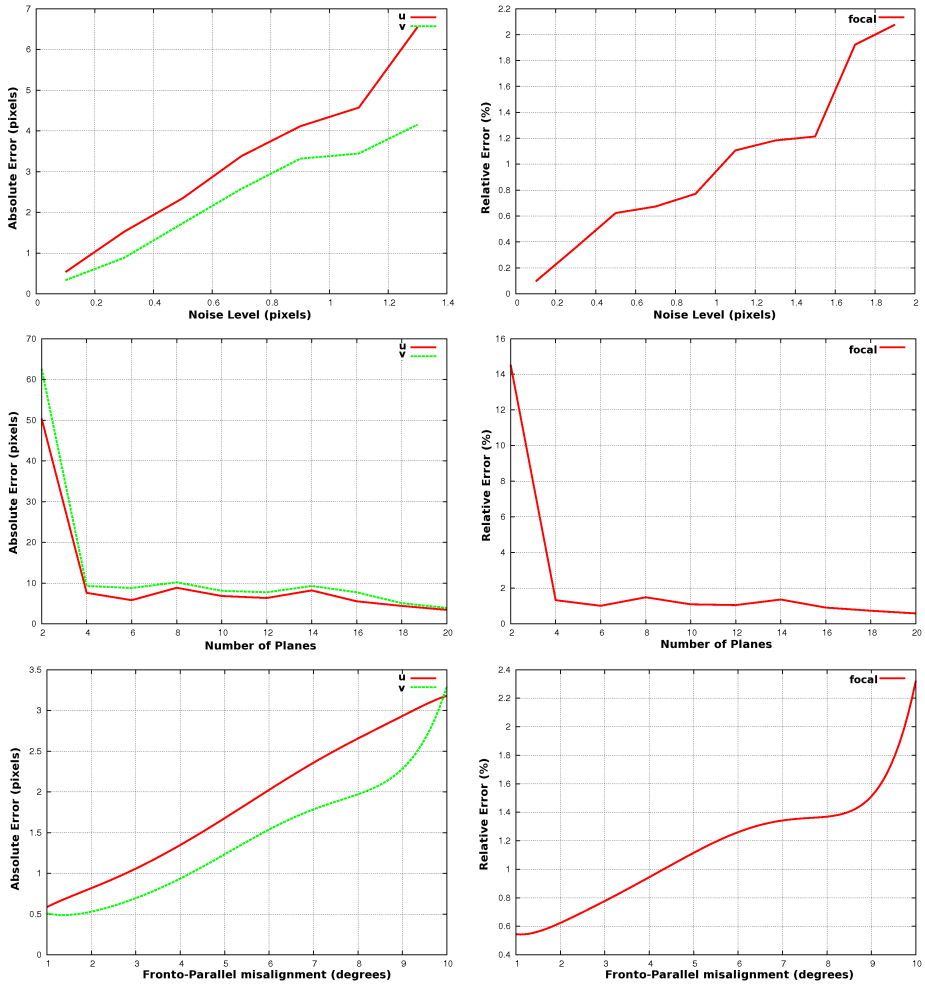

Fig. 3 Results of the synthetic tests on the auto-calibration method. Top, sensitivity to noise level. Middle, sensitivity to number of calibration planes. Bottom, errors regarding the fronto-parallelism inaccuracy. Reported parameters are focal length and principal point (u, v).

6 Conclusion

In this paper we presented two new video projector calibration methods. Both methods alleviate common limitations and requirements of existing methods, like the need for a physical calibration grid and the full knowledge of the camera parameters. We believe that these features of our methods increase their stability, otherwise the error of the camera calibration and/or the detection of printed features would affect the accuracy of the projector calibration.

Each of the presented methods handles these limitation in a different manner. The first method makes reasonable assumptions on the camera whereas the second method rely on the existence of a fronto-parallel pose of the projector.

Very simple to implement, the proposed methods are fast, give good results as reported by our experiments. Moreover, we believe that our methods will improve the calibration of large projectors which were previously hard to calibrate due to cumbersome calibration chessboards required by previous methods.

References

1. Audet, S., Okutomi, M.: A user-friendly method to geometrically calibrate projector-camera systems. In: Proceedings of the IEEE International Workshop on Projector-Camera Systems. Miami Beach, USA (2009)
2. Barsky, S., Petrou, M.: The 4-source photometric stereo technique for three-dimensional surfaces in the presence of highlights and shadows. IEEE Transactions on Pattern Analysis and Machine Intelligence **25**(10), 1239–1252 (2003). DOI http://doi.ieeecomputersociety.org/10.1109/TPAMI.2003.1233898
3. Draréni, J., Sturm, P., Roy, S.: Projector calibration using a markerless plane. In: Proceedings of the International Conference on Computer Vision Theory and Applications, Lisbon, Portugal, vol. 2, pp. 377–382 (2009). URL http://perception.inrialpes.fr/Publications/2009/DSR09
4. Gurdjos, P., Sturm, P.: Methods and geometry for plane-based self-calibration. In: Proceedings of the IEEE Conference on Computer Vision and Pattern Recognition, vol. 1, pp. 491–496. IEEE (2003). URL http://perception.inrialpes.fr/Publications/2003/GS03. Madison, Wisconsin
5. Hartley, R.I., Zisserman, A.: Multiple View Geometry in Computer Vision, second edn. Cambridge University Press, ISBN: 0521540518 (2004)
6. Horn, B.K.P.: Robot Vision (MIT Electrical Engineering and Computer Science), mit press ed edn. The MIT Press (1986)
7. Kimura, M., Mochimaru, M., Kanade, T.: Projector calibration using arbitrary planes and calibrated camera. Computer Vision and Pattern Recognition, IEEE Computer Society Conference on **0**, 1–2 (2007). DOI http://doi.ieeecomputersociety.org/10.1109/CVPR.2007.383477
8. Knuth, D.E.: Art of Computer Programming, Volume 2: Seminumerical Algorithms (3rd Edition). Addison-Wesley Professional (1997)
9. Lee, J.C., Dietz, P.H., Maynes-Aminzade, D., Raskar, R., Hudson, S.E.: Automatic projector calibration with embedded light sensors. In: Proceedings of the 17th annual ACM symposium on User interface software and technology, pp. 123–126. ACM (2004)
10. Lourakis, M., Argyros, A.: The design and implementation of a generic sparse bundle adjustment software package based on the levenberg-marquardt algorithm. Tech. Rep. 340, Institute of Computer Science - FORTH, Heraklion, Crete, Greece (2004). Available from `http://www.ics.forth.gr/~lourakis/sba`
11. Malis, E., Cipolla, R.: Camera self-calibration from unknown planar structures enforcing the multi-view constraints between collineations. IEEE Transactions on Pattern Analysis and Machine Intelligence **4**(9) (2002)
12. Marsaglia, G.: Choosing a point from the surface of a sphere. **43**, 645–646 (1972)
13. Min-Zhi Shao, N.B.: Spherical sampling by archimedes' theorem. Technical Report 184, University of Pennsylvania (1996)
14. Muller, M.E.: A note on a method for generating points uniformly on n-dimensional spheres. **2**, 19–20 (1959)
15. Okatani, T., Deguchi, K.: Autocalibration of a projector-camera system. Pattern Analysis and Machine Intelligence, IEEE Transactions on **27**(12), 1845–1855 (2005). DOI 10.1109/TPAMI.2005.235
16. Ouellet, J.N., Rochette, F., Hébert, P.: Geometric calibration of a structured light system using circular control points. In: 3D Data Processing, Visualization and Transmission, pp. 183–190 (2008)
17. Raij, A., Pollefeys, M.: Auto-calibration of multi-projector display walls. pp. 14–17 Vol.1 (2004). DOI 10.1109/ICPR.2004.1333994
18. Sadlo, F., Weyrich, T., Peikert, R., Gross, M.: A practical structured light acquisition system for point-based geometry and texture. In: Proceedings of the Eurographics Symposium on Point-Based Graphics, pp. 89–98 (2005)
19. Salvi, J., Pagés, J., Batlle, J.: Pattern codification strategies in structured light systems. Pattern Recognition **37**(4), 827–849 (2004)
20. Shen, T., Meng, C.: Digital projector calibration for 3-d active vision systems. Journal of Manufacturing Science and Engineering **124**(1), 126–134 (2002)
21. Sturm, P., Maybank, S.: On plane-based camera calibration: A general algorithm, singularities, applications. In: Proceedings of the IEEE Conference on Computer Vision and Pattern Recognition, Fort Collins, USA, pp. 432–437 (1999). URL http://perception.inrialpes.fr/Publications/1999/SM99a

22. Tao, J.: Slide projector calibration based on calibration of digital camera. In: Society of Photo-Optical Instrumentation Engineers (SPIE) Conference Series, *Presented at the Society of Photo-Optical Instrumentation Engineers (SPIE) Conference*, vol. 6788 (2007). DOI 10.1117/12.774689
23. Triggs, B.: Autocalibration from planar scenes. In: Proceedings of the 5th European Conference on Computer Vision, Freiburg, Germany (1998)
24. Woodham, R.J.: Photometric Stereo: A Reflectance Map Technique for Determining Surface Orientation from a Single View. In: Proceedings of the 22nd SPIE Annual Technical Symposium, vol. 155, pp. 136–143. San Diego, California, USA (1978)
25. Yershova, A., LaValle, S.M.: Deterministic sampling methods for spheres and so(3). In: ICRA, pp. 3974–3980 (2004)
26. Zhang, Z.: Flexible camera calibration by viewing a plane from unknown orientations. Computer Vision, 1999. The Proceedings of the Seventh IEEE International Conference on **1**, 666–673 vol.1 (1999)